Hamburger Beiträge
zur Angewandten Mathematik

Solidification of a GaAs melt - Optimal control of the phase interface

Michael Hinze and Stefan Ziegenbalg

Nr. 2008-06
July 2008

Solidification of a GaAs melt – Optimal control of the phase interface

Michael Hinze[1] and Stefan Ziegenbalg[2]

July 20, 2008

[1] University of Hamburg, Department of Mathematics, D-20146 Hamburg, Bundesstrasse 55, Germany

[2] TU Dresden, Institute of Mathematics, D-01062 Dresden, Zellescher Weg 12-14, Germany

Abstract. We present an optimal control approach for the crystallization of a GaAs melt in a VGF configuration. The solidification process is described by a two phase Stefan problem including flow driven by convection and Lorentz forces. The interface between the liquid and the solid phase is modelled as a graph.

The control goal consists in tracking a prescribed shape and evolution of the free boundary (phase interface) using the crucible temperature and/or Lorentz forces. In particular we intend to achieve a flat free boundary in order to keep the density of dislocations small, compare e.g. [8].

We achieve this goal by minimizing an appropriate cost functional. The resulting optimization problem is solved numerically using an adjoint approach.

In the present work we apply the concept developed in [2, 3, 13] to growth from a melt to a practically relevant configuration [6]. Among other things we show that both, the control with Lorentz forces as well as the control with crucible wall temperature may be applied to achieve the control goal.

1 Introduction

Gallium Arsenide (GaAs) is a semiconductor material with increasing importance. The high electron mobility recommend GaAs in high frequency applications such as transmitting and receiving circuits in mobile phones. GaAs is also very important in optoelectronic, especially for the production of Lasers, LED's, and highly specialised solar panels (e.g. for satellites). GaAs mono crystals are grown using the LEC (Liquid Encapsulated Czochralski) method or the VGF (Vertical Gradient Freeze) method, see [4] for a comparison.

The structural quality of the crystals is strongly influenced by the amount and the distribution of dislocations of the crystal structure which are mainly caused by thermomechanical stress at the phase interface, These tensions can be reduced by a small radial temperature gradient, [6, 8]. Because the temperature gradients occurring with the VGF method are usually small, crystals grown with this technique show a very small dislocation density in comparison to LEC grown crystals, [8].

Assuming that the temperature at the free boundary is constant (equal to melting temperature), the free boundary must become flat in order to eliminate the radial temperature gradient at the free boundary. Thus, our control goal consists in achieving a flat free boundary. In addition to that, we also consider the direct reduction of the radial temperature gradient.

We emphasize that the control approach developed in the present work also allows to increase the crystallization speed of the VGF method while keeping the quality of the crystal.

The mathematical model used in this work governs heat conduction in the solid phase and heat conduction, heat transport and flow in the liquid phase. The two phases are coupled through the Stefan condition and the melting temperature condition at the free boundary. A third order boundary condition models heat transfer between the phases and the crucible wall.

The mathematical approach used in the presented work is described in [2, 3, 13], where solidification of Aluminium is considered as test configuration, and where also a detailed discussion about the related literature [5, 12, 11] can be found.

The results of the numerical experiments are presented in Section 3. There we consider a cylindrical crucible with a GaAs melt and a diameter of $D = 5\,\mathrm{cm}$ and a height of $10\,\mathrm{cm}$. This configuration is relevant at least for experiments considered [6]. Our control goal is to obtain a flat free boundary with a velocity of $5\,\frac{\mathrm{cm}}{\mathrm{h}}$. The results presented in Section 3 strongly differ from the results presented in [3]. This is due to the fact that the physical properties of GaAs strongly differ from that of aluminium.

2 Problem definition

2.1 Mathematical model

Let $\Omega = G \times H$ be a cylindrical domain containing the substance, where G denotes the bottom domain and $H \subset \mathbb{R}$ the height, see Figure 1. The crucible wall, i.e. the boundary of Ω, is denoted by $\partial\Omega$. The time dependent domains $\Omega_s(t)$ and $\Omega_l(t)$ denote the solid and the liquid phase and satisfy $\Omega_s(t) \cup \Omega_l(t) = \Omega$ The free boundary Γ (the phase interface) is described as a graph

$$\Gamma(t) = \left\{ \begin{pmatrix} y \\ f(t,y) \end{pmatrix} : y \in G \right\}$$

with $f : G \to H$. Figure 1 depicts such a configuration.

As mathematical model for the temperatures $u_{s/l}$ in the solid and liquid phase respectively, the velocity $\boldsymbol{v}$ and the pressure p we take

$$\partial_t u_s = \frac{k_s}{c_s \rho} \Delta u_s \qquad \text{in } (0,T] \times \Omega_s, \quad (1)$$

$$\partial_t u_l + \boldsymbol{v} \cdot \nabla u_l = \frac{k_l}{c_l \rho} \Delta u_l \qquad \text{in } (0,T] \times \Omega_l, \quad (2)$$

$$\nabla \cdot \boldsymbol{v} = 0 \qquad \text{in } (0,T] \times \Omega_l, \quad (3)$$

$$\partial_t \boldsymbol{v} + (\nabla \boldsymbol{v})\boldsymbol{v} - \frac{\varepsilon}{\rho} \Delta \boldsymbol{v} + \frac{1}{\rho} \nabla p = -\boldsymbol{g}\gamma(u_l - u_M) + \boldsymbol{A} \qquad \text{in } (0,T] \times \Omega_l, \quad (4)$$

$$L\rho\frac{f_t}{\sqrt{1+f_r}}\frac{k_s}{\rho}\partial_{\boldsymbol{\mu}}u_s\circ\Phi-\frac{k_l}{\rho}\partial_{\boldsymbol{\mu}}u_l\circ\Phi \qquad \text{for } (0,T]\times G, \tag{5}$$

$$\text{with } \Phi(t,y):=\begin{pmatrix} t,\begin{pmatrix} y \\ f(t,y)\end{pmatrix}\end{pmatrix}$$

$$u_s\circ\Phi=u_l\circ\Phi=u_M \qquad \text{on } (0,T]\times G \tag{6}$$

with the initial conditions

$$u_{s/l}(0,\boldsymbol{x})=u_{s/l0}(x) \qquad \text{for } \boldsymbol{x}\in\Omega, \tag{7}$$

$$\boldsymbol{v}(0,\boldsymbol{x})=\boldsymbol{v}_0(x) \qquad \text{for } \boldsymbol{x}\in\Omega, \tag{8}$$

$$f(0,y)=f_0(y) \qquad \text{for } y\in G \tag{9}$$

and the boundary conditions

$$\frac{k_{s/l}}{\alpha_{s/l}}\partial_{\boldsymbol{\nu}}u_{s/l}=u_b-u_{s/l} \qquad \text{on } (0,T]\times\partial\Omega, \tag{10}$$

$$u_{b,\min}\le u_b\le u_{b,\max} \qquad \text{on } (0,T]\times\partial\Omega, \tag{11}$$

$$\boldsymbol{v}=0 \qquad \text{on } (0,T]\times\partial\Omega, \tag{12}$$

$$\partial_{\boldsymbol{\nu}}p=\rho\boldsymbol{\nu}\cdot\big(\boldsymbol{A}-\boldsymbol{g}\gamma(u_l-u_M)\big)+\varepsilon\partial^2_{\boldsymbol{\nu}}v_{\boldsymbol{\nu}} \qquad \text{on } (0,T]\times\partial\Omega_l. \tag{13}$$

Here $\boldsymbol{A}(t,x)$ denotes an external force and $u_b(t,x)$ denotes the crucible wall temperature. These functions serve as control and are described in detail in 2.1.1.

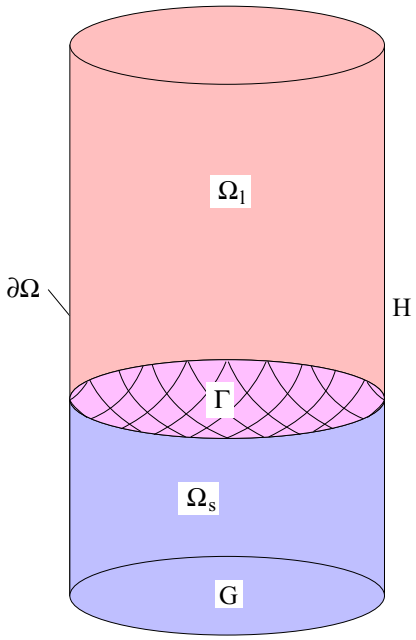

Figure 1: Solid phase Ω_s, liquid phase Ω_l and free boundary Γ in a crucible $\partial\Omega$.

The vector $\boldsymbol{\nu}$ denotes the outer normal vector at the boundary and $\boldsymbol{\mu}$ denotes the normal vector at the free boundary, pointing from the solid to the liquid phase (i.e. $\boldsymbol{\mu} = \boldsymbol{\nu}|_{\partial\Omega_s} = -\boldsymbol{\nu}|_{\partial\Omega_l}$ on Γ).

Equations (3) and (4) form the Navier Stokes equations for incompressible flow, where ε denotes the dynamic viscosity and ρ denotes the density. The buoyancy force is modelled with the Boussinesq approximation by the term $-\boldsymbol{g}\gamma(u_l - u_M)$ using the gravitational force $\boldsymbol{g}$ and the thermal expansion coefficient γ. The external force $\boldsymbol{A}$ is used later in this section to model the Lorentz force.

Equations (1) and (2) are the heat equation in the solid phase and the heat equation with heat transport in the liquid phase, respectively. The constants $k_{s/l}$ and $c_{s/l}$ denote the heat conductivities and the heat capacity in the solid and liquid phase, respectively.

The graph formulation of the Stefan condition (5) is derived in [2, (6)]. The Stefan condition is a conservation law at the free boundary which balances the heat transported into the free boundary and the melting heat generated through solidification. The constant L denotes the latent heat and V_Γ denotes the velocity of the free boundary into normal direction $\boldsymbol{\mu}$.

Equation (6) states the melting temperature condition, where u_M is the melting temperature.

The boundary condition (10) for the temperature follows directly from the heat transfer equation $q = \alpha_{s/l}(u_{s/l} - u_b)$ and the heat conduction $q = k_{s/l}\partial_\nu u_{s/l}$, where q is the heat flow and $\alpha_{s/l}$ is the heat transfer coefficient between the crucible wall and the solid/liquid phase, respectively. The crucible temperature u_b is constrained by (11).

2.1.1 Modeling the control functions

For the modeling of the Lorentz forces we consider a hypothetical rotational symmetric configuration with $G = \{(g_1, g_2) : g_1^2 + g_2^2 \leq R^2\}$ and $h \in H = [h_a, h_b]$ as sketched in Figure 2. This configuration consists of actuator rings of the thickness $dh \to 0$. Each ring consists of an alternating arrangement of electrodes and magnets and each ring can be controlled separately. We assume that the Lorentz force of each ring is rotational symmetric and acts only in tangential direction, see Figure 3. This allows to assemble the total Lorentz force at $\boldsymbol{x} = (g_1, g_2, h)$ by integration over the Lorentz forces generated by each ring

$$\boldsymbol{A}(\boldsymbol{x}) = \int_H A_c(y)\boldsymbol{\tau}(x,y)g\big(\sqrt{(R-r)^2 + (h-y)^2}\big)dy \tag{14}$$

where

$$\boldsymbol{\tau} = \frac{\left((h-y)\frac{g_1}{R}, (h-y)\frac{g_2}{R}, (R-r)\right)}{\sqrt{(R-r)^2+(h-y)^2}} \ , \tag{15}$$

is the tangential vector and A_c is the control force. The function $g(r)$ denotes the dependency of the Lorentz force from the distance d, see Figure 3. We choose

$$g(d) = \frac{e^{-d\frac{\pi}{a}}}{2\sqrt{d}} \ .$$

With this choice for g and $A_c = \text{const.}$ we obtain wall-parallel Lorentz forces in h-direction which satisfy the approximation

$$A(\boldsymbol{x}) \approx A_c e^{-\frac{\pi}{a}\,\mathrm{dist}(\boldsymbol{x}, \partial G \times H)} \ ,$$

compare [1, Appendix] and [10, Section 2,4]. Here a denotes the width of the electrodes and magnets. We note, that effects caused by induction are not taken into account. This makes sense for weakly conductive fluids and partially also for semiconductors or even for high conductive fluids, if we use small magnetic and strong electric fields. Let us note that highly conductive fluids combined with strong electric fields would cause a considerable heating of the material near the crucible wall, which is not considered in our model.

Let $\overline{f}$ be the desired evolution of the free boundary. We consider the rotational symmetric case, i.e. $G = \left\{(g_1, g_2) : g_1^2 + g_2^2 \leq R^2\right\}$ and $h \in H =$

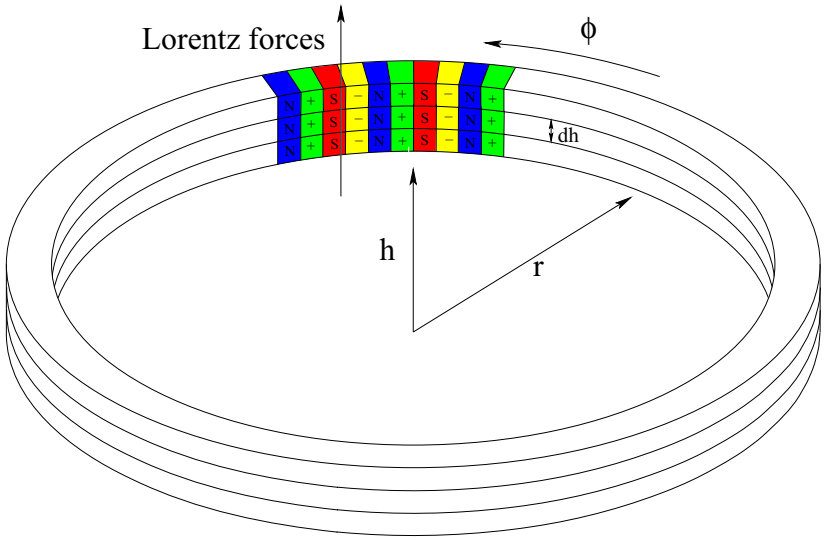

Figure 2: Configuration of actuator rings used for generating Lorentz forces.

$[h_a, h_b]$. As presented in [13], we specify additional boundary conditions for the intersection of the free boundary and the crucible wall;

$$f(t,R) = \overline{f}(t,R) \qquad f_r(t,R) = \overline{f}_r(t,R) = 0 \tag{16}$$

This choice simplifies our moving grid implementation and especially avoids the need of an additional boundary grid for the crucible wall temperature u_b, and thus the interpolation of u_b between two grids. Further details are given in [13].

The boundary conditions (16) induce the following compatibility conditions, which are derived in [13]:

$$L\rho \frac{\overline{f}_t \overline{f}_r}{1+\overline{f}_r^2} = -(\alpha_s - \alpha_l)(u_b \circ \Phi - u_M) \tag{17}$$

$$\left[\alpha_{s/l} \partial_h u_{bs/l}\right]_\Gamma \circ \Phi = \frac{L\rho}{\alpha_s - \alpha_l} f_t \left(\frac{\alpha_l^2}{k_l} - \frac{\alpha_s^2}{k_s}\right) \tag{18}$$

on $(0,T] \times \partial G$. Further we need to ensure that the boundary conditions are satisfied for $t = 0$, i.e., we have to to set

$$u_b(0, \boldsymbol{x}) = u_{s/l0}(\boldsymbol{x}) + \tfrac{k_{s/l}}{\alpha_{s/l}} \partial_\nu u_{s/l0}(\boldsymbol{x}) \ . \tag{19}$$

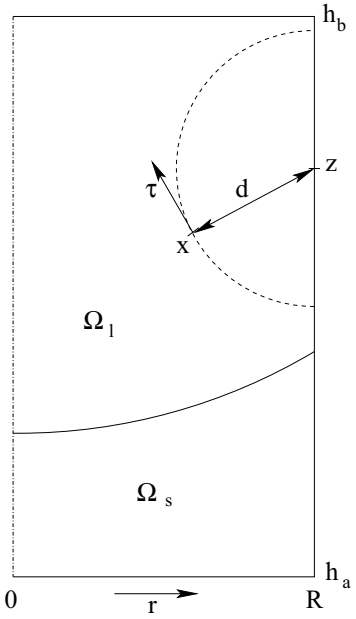

Figure 3: Lorentz forces generated by a single actuator ring.

Since u_b needs to satisfy the compatibility conditions (17) – (19) it cannot serve as control variable directly. We resolve this difficulty by splitting u_b into two parts

$$u_b = u_{b0} + \beta u_{bc} \tag{20}$$

where u_{b0} denotes a fixed part (e.g. a temperature profile known from experience), and βu_{bc} denotes the controllable part, where β is a weight function which allows to tailor the control part of the boundary condition. Now we require that u_{b0} satisfies the compatibility conditions (17) – (19). To ensure this we set

$$\begin{aligned} &\beta(t,\boldsymbol{x}) = \partial_h \beta(t,\boldsymbol{x}) = 0 \qquad && \text{for } \boldsymbol{x} \in \partial\Omega \cap \Gamma \text{ and } t \in (0,T], \\ &\beta(0,\boldsymbol{x}) = 0 && \text{for } \boldsymbol{x} \in \partial\Omega. \end{aligned} \tag{21}$$

With these settings u_b for every choice of u_{bc} satisfies (17) – (19), so that u_{bc} may serve as the control variable in our optimization problem specified below.

2.2 Optimization Problem

Our goal consists in controlling the free boundary using the temperature on the crucible wall and/or near-wall Lorentz forces. As control horizon we take $(0,T]$ for some $T > 0$. Using the desired evolution of the free boundary $\overline{f}$ we define the optimization problem

$$\begin{aligned} J(f, u_{bc}, \boldsymbol{A}_c) :=& \frac{1}{2T} \int_0^T \int_G \big(f(t,y) - \overline{f}(t,y)\big)^2 dy dt \\ &+ \frac{\lambda_T}{2} \int_G \big(f(T,y) - \overline{f}(T,y)\big)^2 dy + \frac{\lambda_S}{2} \int_0^T \int_G (\partial_r u_l)^2 \circ \Phi \qquad (22) \\ =& \min_{f, u_{bc}, \boldsymbol{A}_c}! \\ \text{s.t. } &(1) - (13), (14), (20) \quad , \end{aligned}$$

where

$$\Phi(t,y) := \left(t, \begin{pmatrix} y \\ f(t,y) \end{pmatrix}\right)$$

denotes the re-parametrization $[0,T] \times G \to [0,T] \times \Gamma$. The functional J models the objective in our minimization problem, namely the reduction of the deviation between the free boundary and the desired free boundary. With λ_T

the deviation of the free boundary from the desired free boundary at time $t = T$ is weighted. With $\lambda_S > 0$ radial temperature gradients at the free boundary in the liquid phase are penalized in order to reduce radial temperature gradients directly. This is meaningful since a small error between the free boundary f and a desired flat free boundary $\overline{f}(t, y) = \overline{f}(t)$

$$\int_0^T \int_G (f(t, y) - \overline{f}(t))^2 dy dt$$

does not necessarily result in small radial temperature gradient (, i.e. if the free boundary is wavy).

The functions u_{b0}, β, $\overline{f}$, u_0, f_0 and $\boldsymbol{v}_0$ are given and the functions u, f, $\boldsymbol{v}$ and u_{bc} and/or A_c are sought. From here onwards we assume that the optimization problem admits a solution $(u^*_{s/l}, f^*, \boldsymbol{v}^*, u^*_{bc}, A^*_c)$. Further we assume that the state equations (1) – (13), (14), (20) for every (u_{bc}, A_c) admit a unique solution so that in particular $f = f(u_{bc}, A_c)$. It then is meaningful to replace (22) by

$$K(u_{bc}, \boldsymbol{A}_c) := J\big(f(u_{bc}, \boldsymbol{A}_c), u_{bc}, \boldsymbol{A}_c\big) = \min_{u_{bc}, \boldsymbol{A}_c}! \ , \tag{23}$$

where K denotes the reduced functional. To solve this optimization problem numerically in Section 2.3 we apply a gradient algorithm with an appropriate step size rule. Thus we need an expression for $\nabla K(u_{bc}, \boldsymbol{A}_c)$. It is shown in [3] that for the control using the crucible wall temperature

$$\nabla_{u_{bcs/l}} K(t, x) = -\alpha_{s/l} \beta(t, x) \omega_{s/l}(t, x) \tag{24}$$

holds, and for the control using near-wall Lorentz forces

$$\nabla_{A_c} K(t, y) = -\int_{\Omega_l} \boldsymbol{\psi}(t, x) \cdot \boldsymbol{\tau}(x, y) g\big(\sqrt{(R - r)^2 + (h - y)^2}\big) dx \ , \tag{25}$$

is valid, where $\boldsymbol{x} = (g_1, g_2, h)$, and the tangential vector $\boldsymbol{\tau}$ is defined as in (15). For given u_{bc} and A_c the functions $\omega_{s/l}$ and $\boldsymbol{\psi}$ are obtained by first solving (1) – (13), (14), (20) for u, $\boldsymbol{v}$ and f, and then with these quantities at hand, by solving the so called adjoint system

$$-\partial_t \omega_s = \frac{k_s}{c_s \rho} \Delta \omega_s \qquad \text{in } [0, T) \times \Omega_s, \tag{26}$$

$$-\partial_t \omega_l = \boldsymbol{v} \cdot \nabla \omega_l + \frac{1}{c_l \rho} \big(k_l \Delta \omega_l - \gamma \boldsymbol{g} \cdot \boldsymbol{\psi}\big) \text{in } [0, T) \times \Omega_l, \tag{27}$$

$$k_{s/l}\partial_{\boldsymbol{\nu}}\omega_{s/l} = -\alpha_{s/l}\omega_{s/l} \qquad \text{in } [0,T)\times\partial\Omega, \tag{28}$$

$$\omega_{s/l}(T,x) = 0 \qquad \text{for } x\in\Omega, \tag{29}$$

$$\varphi = -\omega_s\circ\Phi = -\omega_{s/l}\circ\Phi - \frac{\lambda_S f_r^2\partial_{\boldsymbol{\mu}}u_l}{k_l(1+f_r^2)^{1.5}}\circ\Phi \qquad \text{for } t\in(0,t),\ y\in G, \tag{30}$$

$$\nabla\cdot\boldsymbol{\psi} = 0 \qquad \text{in } (0,T]\times\Omega_l, \tag{31}$$

$$\boldsymbol{\psi} = 0 \qquad \text{in } (0,T]\times\partial\Omega_l, \tag{32}$$

$$-\partial_t\boldsymbol{\psi} - (\nabla\boldsymbol{\psi}^T)\cdot\boldsymbol{v} + (\nabla\boldsymbol{v}^T)\boldsymbol{\psi} - \frac{\varepsilon}{\rho}\Delta\boldsymbol{\psi} \tag{33}$$

$$= -c_l\rho\omega_l\nabla u_l + \nabla\pi \qquad \text{in } [0,T)\times\Omega_l, \tag{34}$$

$$\boldsymbol{\psi}(T,x) = 0 \qquad \text{for } x\in\Omega_l, \tag{35}$$

$$\partial_{\boldsymbol{\nu}}\pi = \partial_{\boldsymbol{\nu}}u c_l\rho\omega_l - \varepsilon\partial^2_{\boldsymbol{\nu}}\boldsymbol{\psi}_{\boldsymbol{\nu}} \qquad \text{in } [0,T)\times\partial\Omega_l, \tag{36}$$

$$\begin{aligned} -L\rho\partial_t\varphi = {} & \frac{\overline{f}-f}{T} - f_r^2\partial_h u_l\partial_h^2 u_l\circ\Phi \\ & + \partial_r\big(f_r(\partial_h u_l)^2\circ\Phi\big) + \frac{f_r}{r}\big((\partial_h u_l)^2\circ\Phi\big) \\ & - L\rho\partial_r\left(\frac{2\varphi f_r f_t}{1+f_r^2}\right) - L\rho\frac{2\varphi f_r f_t}{r(1+f_r^2)} \\ & - \varphi(1+f_r^2)[k_{s/l}\partial_h^2 u_{s/l}]_\Gamma\circ\Phi \\ & - \big[k_{s/l}\partial_{\boldsymbol{\mu}}\omega_{s/l}\partial_{\boldsymbol{\mu}}u_{s/l}\big]_\Gamma\circ\Phi \qquad \text{in } [0,T)\times G, \end{aligned} \tag{37}$$

$$L\rho\varphi(T,y) = \lambda_T\big(\overline{f}(T,y) - f(T,y)\big) \qquad \text{on } y\in G. \tag{38}$$

For a detailed derivation of adjoint system and its connection to ∇K we refer the reader to [9].

2.3 The numerical approach

For the solution of the optimization problem

$$K(u_{bc}, A_c) = \min_{u_{bc},A_c}!\ ,$$

we use a projected gradient algorithm with line minimization and a suitable stopping criterion, which is developed in [9]. The PDE systems are discretized on a moving grid using the finite volume technique. The algorithm is implemented using the Open Source toolbox OpenFOAM [7]. A detailed description of the numerical implementation and the CG-Algorithm used to solve the linear sub problems can be found in [13].

3 Numerical results

As the test problem we consider a GaAs melt in a rotational symmetric cylinder with a diameter of 5 cm and a height of 10 cm. The diameter of this test configuration is equal to the diameter for the experimental VGF oven presented in [6]. Thus the domain is described by $\Omega = G \times H$ with the ground $G = \left\{(g_1, g_2) : g_1^1 + g_2^2 \leq R^2\right\}$ with $R = 2.5\,\mathrm{cm}$, and the height $H = [h_a, h_b] = [0, 10\,\mathrm{cm}]$. The solid phase is on the bottom and the liquid phase is on the top. The gravitational force is directed downwards, i.e. $\boldsymbol{g} = \big((0,0), -9.82\big)\,\frac{\mathrm{m}}{\mathrm{s}^2}$.

We optimize the solidification process over the time period $[0, T]$ with $T = 3600\,\mathrm{s}$. We note that the time taken in [3] for the solidification of a similar aluminium configuration is $T = 25\,\mathrm{s}$. This is caused by the fact that the solidification speed of aluminium is much higher than that of GaAs due to the much higher heat conduction of aluminium.

The physical constants for GaAs are

$$\rho = 5170\,\tfrac{\mathrm{kg}}{\mathrm{m}^3} \qquad u_M = 1238\,^\circ\mathrm{C} \qquad L = 726000\,\tfrac{\mathrm{J}}{\mathrm{kg}} \qquad \boldsymbol{g} = \big((0,0), -9.82\big)\,\frac{\mathrm{m}}{\mathrm{s}^2}$$
$$c_l = 434\,\tfrac{\mathrm{J}}{\mathrm{kg}\cdot\mathrm{K}} \qquad k_l = 17.8\,\tfrac{\mathrm{J}}{\mathrm{s}\cdot\mathrm{m}\cdot\mathrm{K}} \qquad \gamma = 1.87 \cdot 10^{-4}\,\tfrac{1}{\mathrm{K}} \qquad \varepsilon = 2.79 \cdot 10^{-3}\,\tfrac{\mathrm{kg}}{\mathrm{m}\cdot\mathrm{s}}$$
$$c_s = 420\,\tfrac{\mathrm{J}}{\mathrm{kg}\cdot\mathrm{K}} \qquad k_s = 7.12\,\tfrac{\mathrm{J}}{\mathrm{s}\cdot\mathrm{m}\cdot\mathrm{K}}$$

For $\alpha_{s/l}$ we choose $\alpha_s = 1000\,\frac{\mathrm{J}}{\mathrm{s}\cdot\mathrm{m}^2\cdot\mathrm{K}}$ and $\alpha_l = 200\,\frac{\mathrm{J}}{\mathrm{s}\cdot\mathrm{m}^2\cdot\mathrm{K}}$. The desired free boundary is the moving plane

$$\overline{f}(t, y) = 2.5\,\mathrm{cm} + 5\,\frac{\mathrm{cm}}{\mathrm{h}}\ .$$

For λ_T (see (22)) we chose $\lambda_T = 0.3$ as in [3].

Several control cases are considered. First, we control using the crucible wall temperature u_b, so that ∇K is given by (24). Secondly, we control using the near-wall Lorentz forces as described in Section 2.1.1 with ∇K given in (25). In the last part of this Section we examine the reduction of radial temperature gradients near the free boundary by setting $\lambda_S > 0$ (see (22)) using crucible wall temperature control and Lorentz force control.

The spatial mesh contains 120 cells in vertical and 30 cells in radial direction, where we recall that symmetry is exploited.

3.1 Results for the uncontrolled case

First we examine the results for the uncontrolled forward problem with $u_{bc} = 0$ and $A_c = 0$. Figure 4 shows the shape of the free boundary, the temperature u and the velocity $\boldsymbol{v}$ in the liquid phase at three different time instances.

The images (e.g. in Figure 4) show colored stripes. Every stripe and color represents a temperature interval corresponding to the legend shown right. The black line depicts the free boundary. The arrows are directed into the direction of the flow and their length is proportional to the magnitude of the velocity.

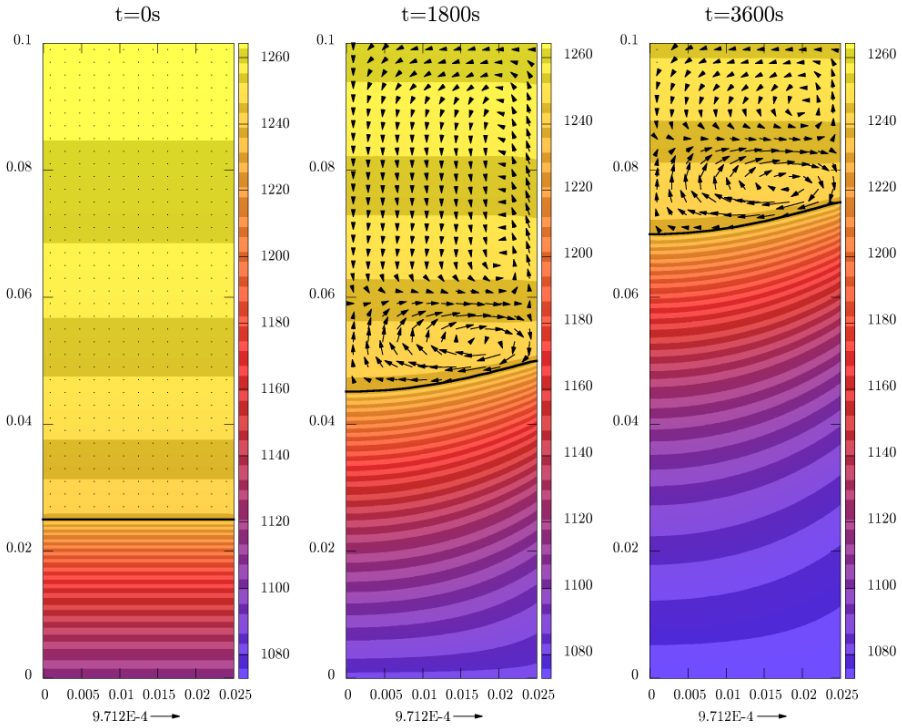

Figure 4: The temperature u (colored stripes), the velocity (arrows) and the free boundary (black line) for the uncontrolled problem for three different time instances.

3.2 Results with crucible wall temperature control

Fist we examine the control with the crucible wall temperature.

Figure 5 shows the shape of the free boundary, the temperature and the velocity at two different time instances with and without control. (The plots for $t = 0$ are omitted, since the temperature and the free boundary for the controlled case and the uncontrolled case are equal.) Figure 6 (red line) presents the evolution of the relative cost functional $J^{(k)}/J^{(0)}$ (see (22)) where k is the gradient iteration. As can be seen this functional is reduced very quickly, and that the optimized evolution of the free boundary delivers a nearly flat graph at all time instances.

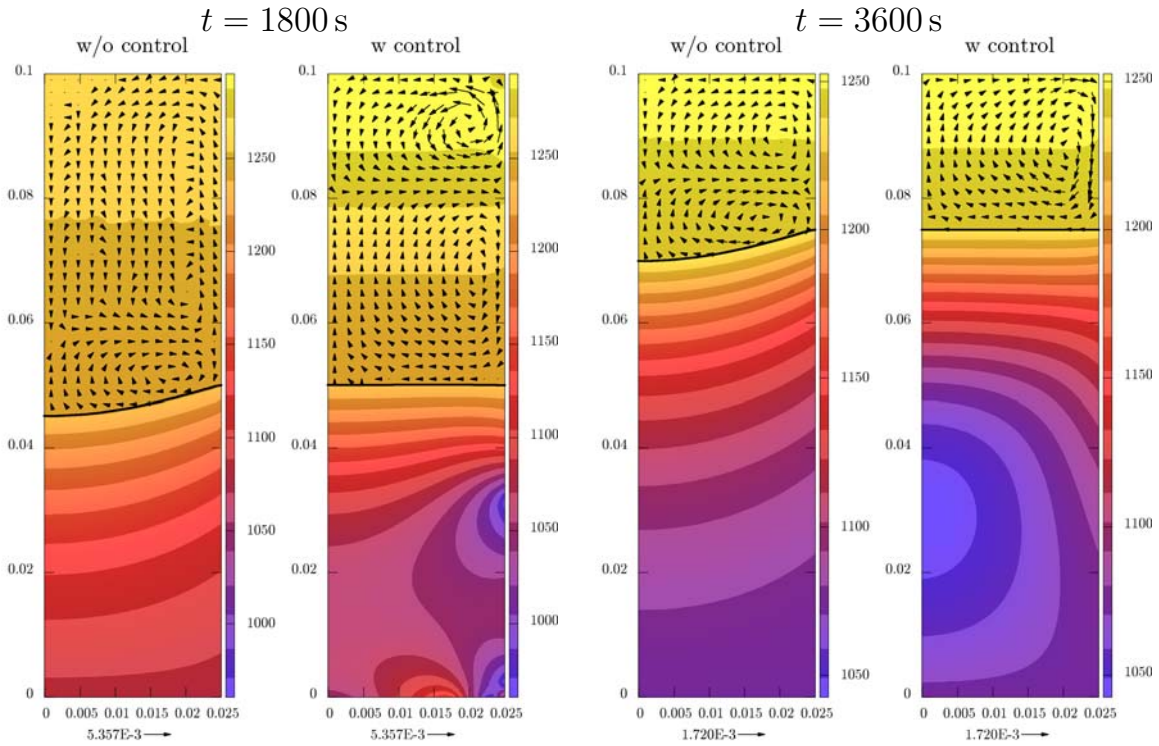

Figure 5: The temperature u (colored stripes), velocity (arrows) and free boundary (black line) with and without control and at two time instances for the problem with crucible wall temperature control.

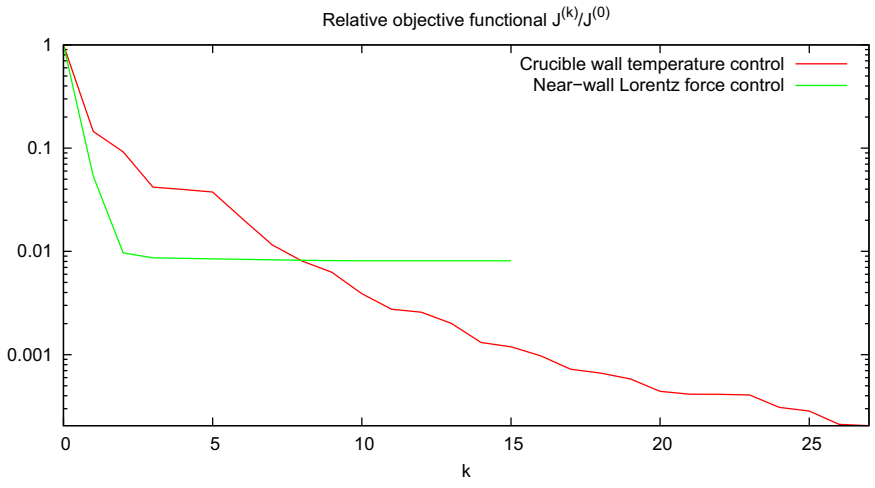

Figure 6: Iteration history of $J^{(k)}/J^{(0)}$ with crucible wall temperature control and with near-wall Lorentz force control. Both cases work but control with crucible wall temperature performs clearly better.

3.3 Results with near wall Lorentz force control

Now we investigate the control with near-wall Lorentz forces. The numerical results are presented in the Figures 7 (temperature, velocity and free boundary) and 6 (cost functional).

As can be seen, the control with Lorentz forces also works well. This is in contrast to the control of solidification of aluminium for a problem of the same size we considered in [3]. There it was not possible track the prescribed flat free boundary. This phenomenon can be explained using Figure 9. The area around the intersection of the free boundary with the crucible wall is the coldest zone in the liquid phase. To achieve a flat free boundary the material sitting in this zone has to be transported to the center (dashed arrow). To achieve this the Lorentz forces should act in the direction sketched in Figure 9. This mechanism is also visible in the numerical experiment shown in Figures 7 and 8, where the Lorentz forces and the velocity in liquid phases are depicted.

But the flow driven by that Lorentz forces (and also by the convection) satisfies $\boldsymbol{v} = 0$ at $\partial\Omega_l$ so that the cold material arrives at the center delayed, i.e. the free boundary is „hanging back".

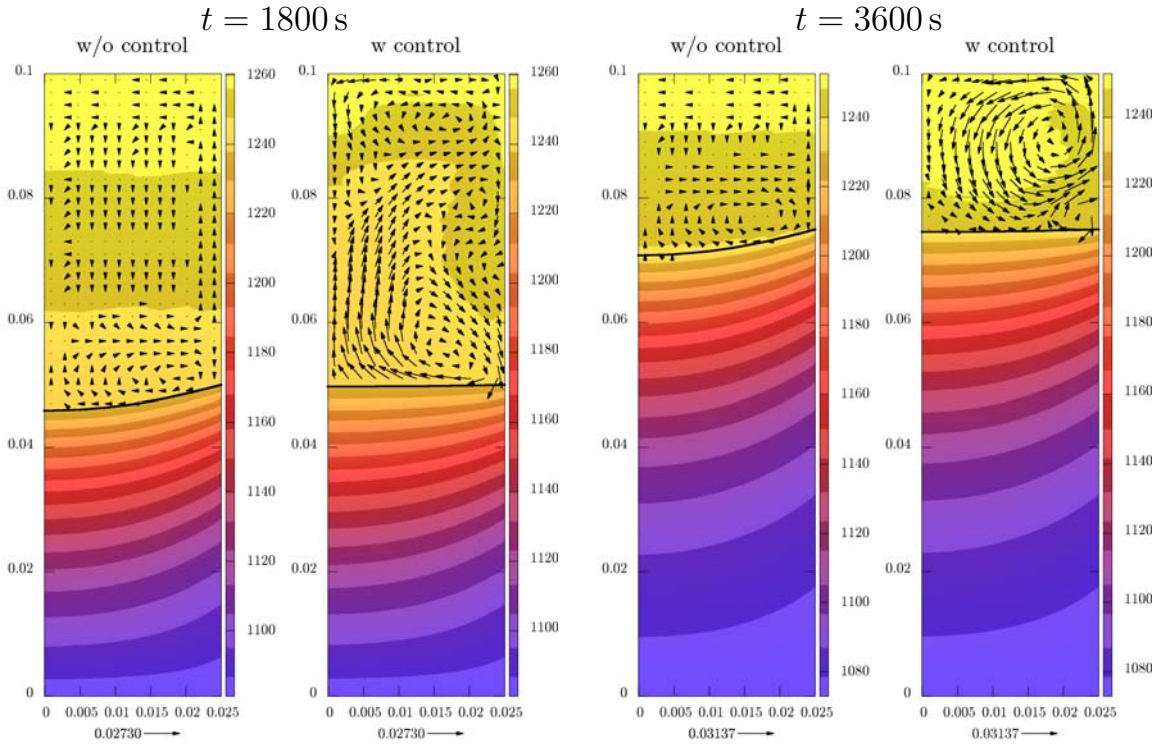

Figure 7: The temperature u (white and grey stripes), velocity (arrows) and free boundary (black line) with and without control and at two time instances for the problem with Lorentz force control.

(If the Lorentz forces would act in the opposite direction as sketched in Figure 9 the material would be heated up at the crucible wall and hot material (instead of cold material) would flow to the center.)

The influence of this effect strongly depends on the crystallization speed. If the free boundary moves slower, i.e. if a certain amount of melt takes more time for crystallization, more cold material can be transported into the center. Since the crystallization speed of the GaAs configuration is 144 times lower than that for the aluminium configuration of equal size considered in [3] (3600 s instead of 25 s) solidification control using Lorentz forces performs much better for GaAs than for aluminium. But the effect described in Figure 9 still occurs, as can be seen in comparison of the cost functionals in Figure 6.

3.4 Reduction of the radial temperature gradient

In this section we demonstrate the reduction of the radial temperature gradient by setting $\lambda_S = 2 \cdot 10^{-7}$. With this choice

$$J_s := \frac{\lambda_S}{2} \int_0^T \int_G (\partial_r u_l)^2 \circ \Phi \tag{39}$$

is approximately twice large as the remaining part of J in (22).

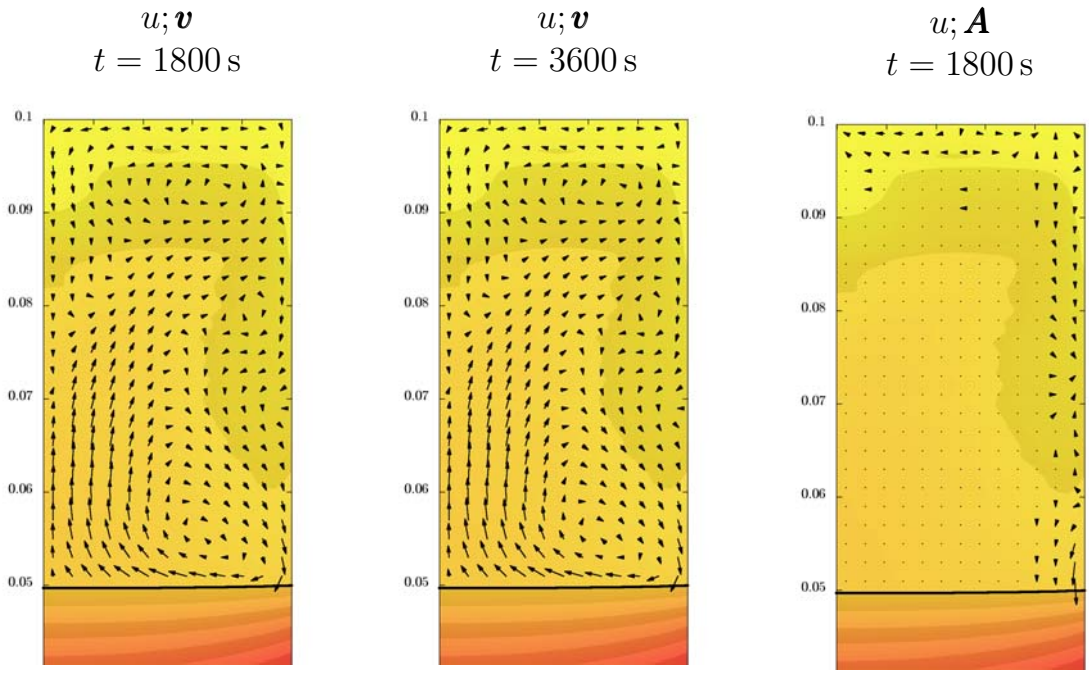

Figure 8: The velocity $\boldsymbol{v}$ and the Lorentz forces $\boldsymbol{A}$ (arrows) in the liquid phase. At the free boundary the Lorentz forces generate a flow directed to the center.

We examine the control using the crucible wall temperature. Except of λ_S the test configuration is equal to the case described in Section 3.2. (Since near wall Lorentz force control delivers similar results, we only consider crucible wall temperature control here.)

Figure 10 shows the results. It can be seen that the primary control goal of tracking the prescribed flat free boundary is achieved still.

Figure 11 shows that the functional J_S which expresses the radial temperature gradient at the free boundary in the liquid phase is reduced approximately twice much as compared to the case with $\lambda_S = 0$.

The green graph in Figure 11 for $\lambda_S = 0$ also shows, that the radial temperature gradient is mainly reduced by the primary control goal, namely the tracking of a flat free boundary. (Due to the melting temperature condition $u = u_M$ at the free boundary the radial temperature gradient is zero, if the free boundary is flat.)

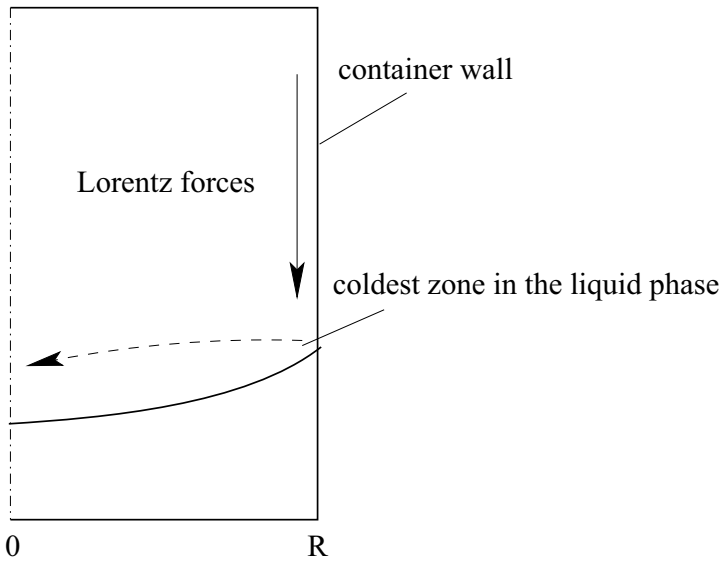

Figure 9: Influence of the flow. In order to achieve a flat free boundary, the cold material must be transported to the center. This is achieved by applying Lorentz forces as depicted. Compare also Figures 8 and 7.

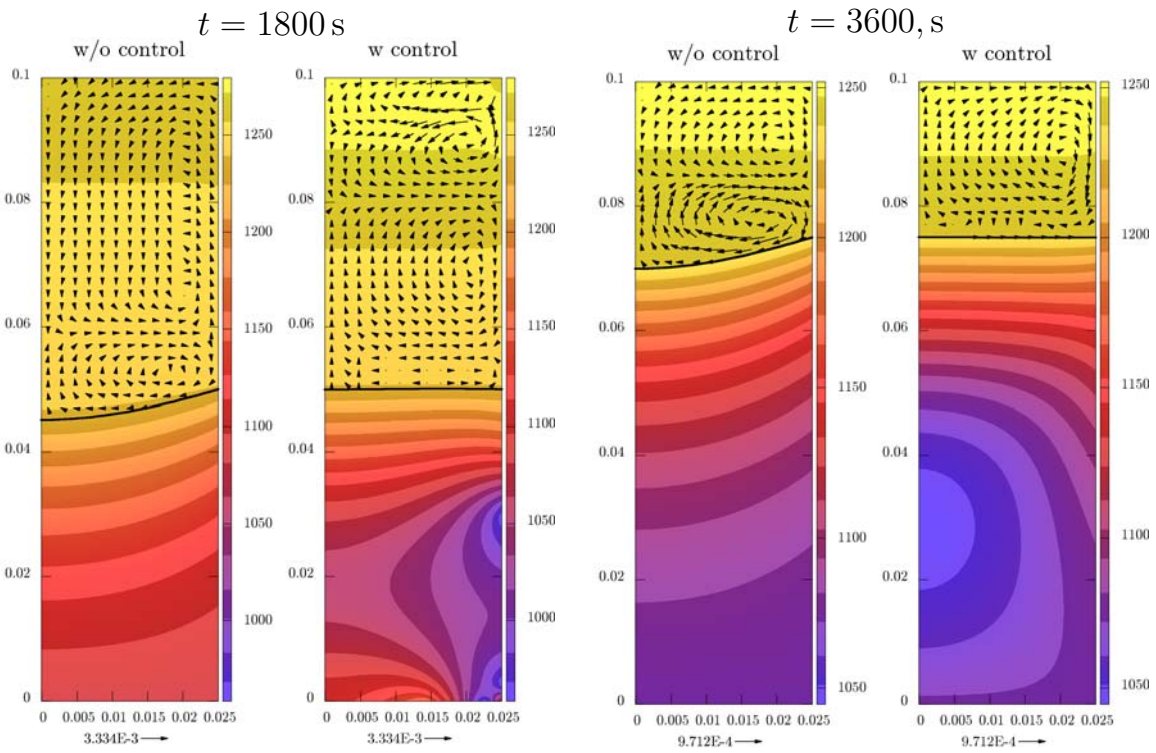

Figure 10: The temperature u (colored stripes), velocity (arrows) and free boundary (black line) with and without control and at two time instances for the problem with crucible wall temperature control and with additional reduction of the radial temperature gradients.

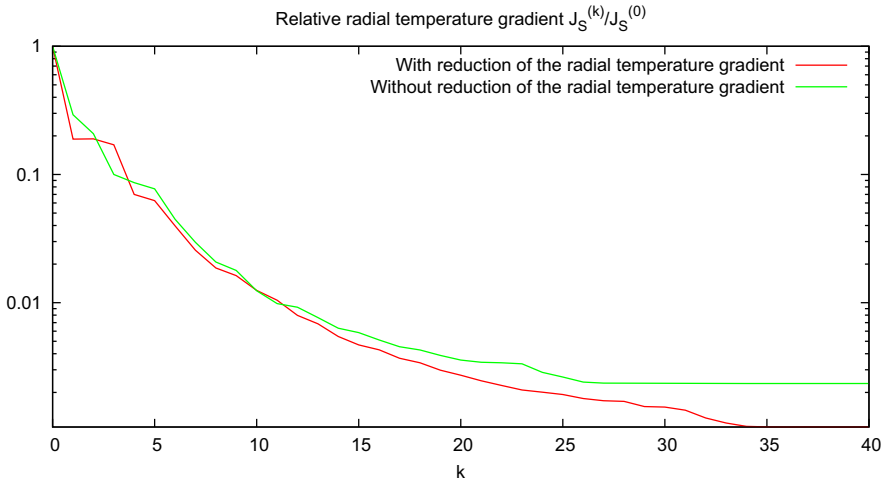

Figure 11: Iteration history of $J_S^{(k)}/J_S^{(0)}$ for each gradient iteration k. With $\lambda_S = 2 \cdot 10^{-7}$ the radial temperature gradient is reduced approximately two times stronger.

Conclusion and prospect

We present a control algorithm for the solidification process within a VGF (Vertical Gradient Freeze) configuration. The primary control goal consists in tracking a prescribed evolution of the phase interface (free boundary). Additionally we also consider reduction of the radial temperature gradients as secondary control goal. As control actions we consider heating the crucible wall and near wall Lorentz forces.

The physical model incorporates flow driven by convection and Lorentz forces, heat conduction and transport, and the Stefan condition at the free boundary.

To demonstrate the scope of our method we numerically examine a GaAs melt. We show, that that both, tracking of the prescribed free boundary and the reduction of the radial temperature gradients works very well using crucible wall temperature control. In contrast to the aluminum test problem considered in [3] the control of the free boundary using near wall Lorentz forces also works well for the GaAs test problem considered here. This is due to the significant lower crystallization speed of GaAs in comparison to aluminium.

Since in practice it is not possible to heat the crucible wall directly in a next step also radiation needs to be considered. Furthermore we intend to consider a different geometry of the crucible wall and different magnetic field configurations for the generation of Lorentz forces. As starting point for our future work we take the experimental configuration described in [6].

References

[1] T.W. Berger, J. Kim, C. Lee, and J. Lim. Turbulent boundary layer control utilising lth Lorentz force. *Physics of Fluids*, 12(3):631–649, 2000.

[2] M. Hinze and S. Ziegenbalg. Optimal control of the free boundary in a two-phase stefan problem. *J. Comput. Phys.*, 223:657–684, 2006.

[3] M. Hinze and S. Ziegenbalg. Optimal control of the free boundary in a two-phase stefan problem with flow driven by convection. *ZAMM*, 87:430–448, 2007.

[4] M. Jurisch, D. Behr, T. Bindemann, T. Bünger, T. Flade, W. Fliegel, R. Hammer, S. Hölzig, A. Kiesel, A. Kleinwechter, A. Köhler, U. Kretzer, A. Seidl, and B. Weinert. State-of-the-art semi-insulating gaas substrates. In *Compound Semiconductors 1999: Proceedings of the 26th International Symposium on Compound Semiconductors*, Berlin, August 1999.

[5] S. Kang and N. Zabaras. Control of the freezing interface motion in two-dimensional solidification processes using the adjoint method. *International Journal for Numerical Methods in Engineering*, 38:63–80, 1995.

[6] H. Krause, O. Pätzold, U. Wunderwald, and M. Herman. Thermally optimized furnace for the growth of single-crystalline semiconductors by the vertical gradient freeze technique. *Elektrowärme-International*, 4:142, 2001.

[7] OpenFOAM: The Open Source CFD Toolbox. http://www.opencfd.co.uk/openfoam/.

[8] P. Rudolph and M. Jurisch. Bulk growth of gaas: An overview. *Journal of crystal growth*, 198/199:325 – 335, 1999.

[9] F. Tröltzsch. *Optimalsteuerung bei partiellen Differentialgleichungen.* Vieweg, 2005.

[10] T. Weier. *Elektromagnetische Strömungskontrolle mit wandparallelen Lorentzkräften in schwach leitfähigen Fluiden.* PhD thesis, Technische Universität Dresden, Fakultät Maschienenwesen, 2005.

[11] Z. Yang. *The adjoint method for the inverse design of solidification processes with convection.* PhD thesis, Cornell University, 1997.

[12] N. Zabaras and T. Hung Nguyen. Control of the freezing interface morphology in solidification processes in the presence of natural convection. *International Journal for Numerical Methods in Engineering*, 38:1555–1578, 1995.

[13] S. Ziegenbalg. *Kontrolle freier Ränder bei der Erstarrung von Kristallschmelzen.* PhD thesis, Technische Universität Dresden, Institut für Numerische Mathematik, 2008.